

Physical modeling of vanishing bores in open-channel flows

Youkai Li and Hubert Chanson

Abstract: When an undular bore propagates upstream against a subcritical flow in a flat channel, its leading front may weaken and vanish. The present study physically investigated the entire decaying process of vanishing bores in a relatively large facility. The invert was made of mobile or fixed natural river gravel. Detailed sampling of water surface elevations and velocities was performed in combination with high-resolution photos and video recordings. Despite some increased turbulence characteristics linked to the bore front arrival, no sediment motion was observed underneath the vanishing bores. The quantitative results provide a unique benchmark dataset for further study of later-stage bore propagations.

Key words: tidal bore, open channel flow, vanishing process, physical modeling.

Résumé : Lorsqu'un mascaret onduleux se propage en amont contre un écoulement sous-critique dans un canal d'écoulement plat, son principal front peut s'affaiblir et disparaître. La présente étude a examiné physiquement l'ensemble du processus d'évanescence des mascarets dans une installation relativement grande. Le radier était constitué de graviers fluviaux naturels mobiles ou fixes. Un échantillonnage détaillé des élévations et des vitesses de surface de l'eau a été effectué au moyen d'enregistrements photo et vidéo à haute résolution. Malgré certaines caractéristiques de turbulence accrue liées à l'arrivée du front du mascaret, aucun mouvement de sédiments n'a été observé sous les mascarets évanescents. Les résultats quantitatifs fournissent un ensemble de données de référence unique pour une étude plus approfondie de la propagation des mascarets à un stade ultérieur. [Traduit par la Rédaction]

Mots-clés : mascaret, écoulement dans un canal à surface libre, processus d'évanescence, modélisation physique.

Introduction

A bore or positive surge is a travelling hydraulic jump in an open channel. Relevant natural and artificial processes encompass tsunami-induced bores (St-Germain et al. 2014), storm-surge-induced bores (Murty et al. 1986), wave run-ups in swash zones (Kobayashi and Johnson 2001), positive surges produced by sudden gate operation in open channels such as navigation canals and hydro-power canals (Treske 1994), as well as tide-induced processes in natural estuaries, such as tidal bores (Fig. 1 and Chanson 2011a). In a rectangular channel, the shape of a bore propagating upstream is intrinsically related to its bore Froude number Fr_1 :

$$(1) \quad Fr_1 = \frac{V_1 + U}{\sqrt{g \times d_1}} = Fr_o + \frac{U}{\sqrt{g \times d_1}}$$

where V_1 is the magnitude of the bulk velocity of the steady inflow downstream, U represents the magnitude of bore travelling speed upstream (relative to an observer standing on the riverbank near the bore front), d_1 denotes the initial water depth, g is the gravitational acceleration, and $Fr_o = V_1 / \sqrt{g \times d_1}$ characterizes the Froude number of the initially steady inflow.

When a bore propagates upstream against a supercritical inflow in a sloping open channel, it may decelerate and evolve into a stationary hydraulic jump, that is, an arrested bore (Chanson 2011b; Li and Chanson 2018; Viero et al. 2017). During the entire transformation process, the bore Froude number progressively decreases but remains larger than unity. On the other hand, when a relatively weak bore propagates against a subcritical inflow, the height of

the bore front may gradually decrease to zero and the bore vanishes. Vanishing bore processes can commonly be observed at the final stage of the decaying tidal bore, for example, the Qiantang Bore near Wenyan (Zeng et al. 2017). However, the hydrodynamics of vanishing bores have rarely been studied by physical modeling because of the challenges in achieving well-controlled and repeatable flow conditions. A few analytical studies have proposed models to describe the positive surges propagating in rectangular channels with simplified assumptions (Li et al. 2017; Viero et al. 2017). These models were compared to limited free-surface observations in laboratory flumes, mostly focusing on the early stage of bore formation and propagation, and the last phase of bore vanishing was not physically recorded.

The current study investigates the vanishing bore process from generation to disappearance, based on laboratory experiments in a relatively large facility. The aim of this study is to document in detail the free-surface and velocity characteristics under carefully controlled flow conditions. This study was part of the PhD project by Li (2020).

Experimental setup

Physical modeling was performed in a 15 m long and 0.5 m wide rectangular tilting channel with transparent tempered glass sidewalls and a PVC bed (Fig. 2), previously used by Li and Chanson (2018). Herein, the channel bed was smooth for $x < 1.50$ m and $x > 13.0$ m, where x indicated the longitudinal distance measured from the upstream end of the test section. For $1.50 \text{ m} < x < 13.0 \text{ m}$, the bed consisted of natural river pebbles sieved between 6.7 mm and 9.5 mm, which provided relatively larger flow resistance and maintained the subcritical flow regime

Received 23 June 2020. Accepted 9 April 2021.

Y. Li and H. Chanson. The University of Queensland, School of Civil Engineering, Brisbane, QLD 4072, Australia.

Corresponding author: Youkai Li (email: youkai.li@uqconnect.edu.au).

© 2021 The Author(s). Permission for reuse (free in most cases) can be obtained from copyright.com.

Fig. 1. A gentle undular bore with some smooth surface undulations and a surfer in the Garonne River (France) on the afternoon of 3 June 2012. The red arrows indicate the leading bore front. [Colour online.]

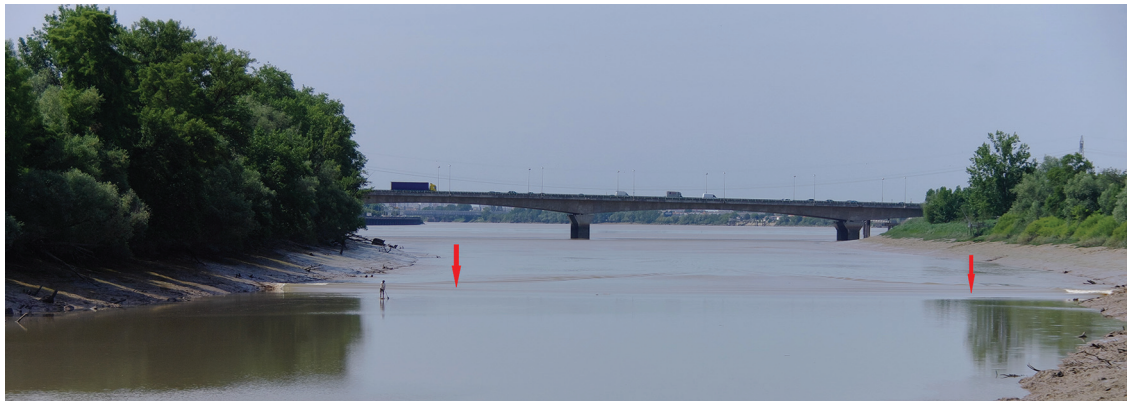


Fig. 2. Experimental flume configuration for the vanishing bore experiments – the vertical coordinate z was measured from the top of the pebble layer. θ : channel tilting angle; V_1 : bulk velocity of initial inflow; d_1 : initial water depth of inflow; U : bore celerity; V_2 : bulk velocity of conjugate flow; d_2 : water depth of conjugate flow; h : Tainter gate opening after closure.

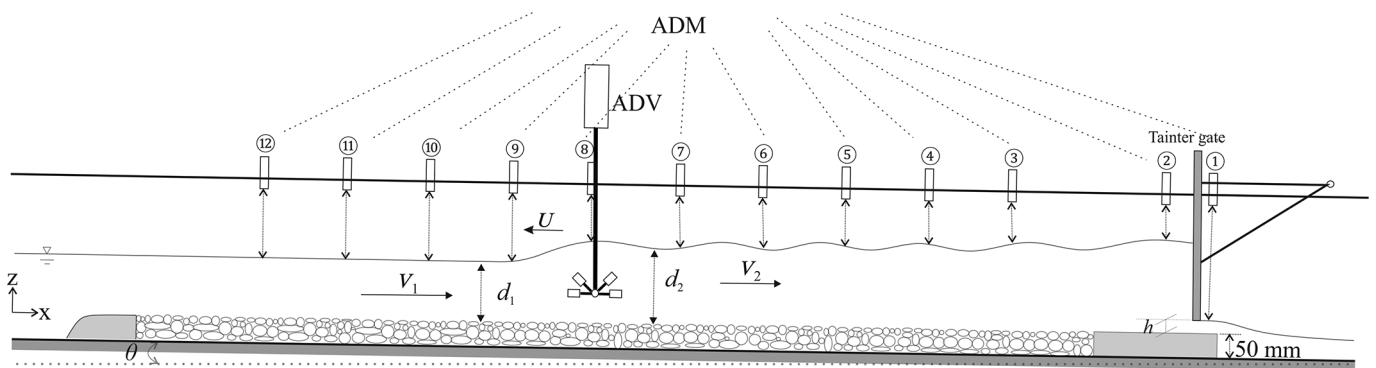


Table 1. Initial flow conditions prior to tidal bore passage on the gravel section in the sloping channel during vanishing bore experiments.

Experiment	Bed type	Fr_0 (–) at different longitudinal locations x (m)									
		12	11	10	9	8	7	6	5	4	3
VB1	Mobile gravel	0.85	0.84	0.79	0.81	0.79	0.72	0.69	0.76	0.80	0.84
VB2	Fixed gravel	0.79	0.75	0.77	0.77	0.74	0.69	0.67	0.73	0.76	0.82

Note: Fr_0 : inflow Froude number; x : longitudinal location measured from the upstream end of the flume.

Table 2. Unsteady flow conditions during the vanishing bore experiments.

Experiment	Bed type	Q (m^3/s)	S_o (–)	h (mm)	Fr_1^* (–)	d_1^* (m)	U^* (m/s)	d_c (m)	V_c (m/s)
VB1	Mobile gravel	0.039	0.0068	63	1.06	0.106	0.34	0.085	0.914
VB2	Fixed gravel	0.039	0.0068	63	1.03	0.108	0.34	0.085	0.914

Note: Q : flow rate; S_o : channel slope ($S_o = \sin \theta$); h : Tainter gate opening after closure; Fr_1 : bore Froude number; d_1 : initial water depth of inflow; U : bore celerity; B : channel width; d_c : critical water depth; $d_c = [Q^2/(g \times B^2)]^{1/3}$; V_c : critical flow velocity; $V_c = Q/(d_c \times B)$.

*These parameters were measured and (or) calculated at $x = 7$ m of the test section.

through this section to ensure the occurrence of vanishing bores. During the first series of experiments, the pebbles were mobile (i.e., free to move), initially distributed randomly, and compacted using a screed (Experiment VB1). In the second series, the same gravel bed was sprayed with a very thin protective coating (NanoProtect SC-96, <0.1 mm), which created a fixed gravel invert (Experiment VB2). The channel slope was $S_o = 0.0068$ for both Experiments VB1 and VB2.

The two series of experiments were conducted under similar flow conditions with a discharge $Q = 0.039 m^3/s$, except for different bed gravel configurations (Tables 1 and 2). The discharge was measured using an onsite calibrated Venturi flowmeter with an accuracy of $10^{-4} m^3/s$. In Experiment VB1, the initial steady flow induced some pebble sorting and a limited amount of downstream-moving loose gravel; that is, the bed was slightly water-worked. In Experiment VB2, no pebble motion occurred. The

Fig. 3. Photographs of propagating and vanishing undular bores: (a) an undular bore (red arrow) shortly after generation propagating from right to left near $x = 13$ m in Experiment VB1; (b) a decelerating undular bore (red arrow) propagating from right to left near $x = 11$ m on the sloping mobile gravel bed before vanishing in Experiment VB1; (c) a vanishing bore (red arrow) propagating from right to left near $x = 5.5$ m on the sloping fixed gravel bed in Experiment VB2. Flow conditions: $Q = 0.039 \text{ m}^3/\text{s}$, $S_o = 0.0068$, $h = 63 \text{ mm}$. [Colour online.]



initial inflow was subcritical throughout the entire gravel bed section (Table 1). On the mobile gravel bed, the initial flow had a slightly higher Froude number than that on the fixed gravel bed at all sampling locations. This should be linked to the slightly organized bed roughness in Experiment VB1 due to water work. The bores were generated by suddenly closing the Tainter gate in less than 0.2 s with a gap below ($h > 0$, as illustrated in Fig. 2). The overall unsteady flow conditions are listed in Table 2.

Twelve acoustic displacement meters (ADMs) Microsonic® Mic+25/IU/TC were installed above the channel centerline at different longitudinal locations, recording the instantaneous free-surface elevations with an error of less than 0.1 mm. An acoustic Doppler velocimetry (ADV) Nortek Vectrino+ was installed at $x = 7$ m to measure the instantaneous velocity (Fig. 2). The accuracy of the flow velocity measurements was $\pm 1\%$ of the measured value of $\pm 1 \text{ mm/s}$. The instantaneous free-surface elevations and flow velocities were measured simultaneously at a sampling rate of 200 Hz. For a given set of flow conditions, the experiment was repeated 25 times to enable the ensemble analysis.

Basic flow patterns: bore propagation and transformation

For the two different sets of bore experiments, visual observation and video camera recording showed a comparable bore shape and vanishing process. The bore slightly broke after generation and immediately became an undular bore with a smooth front when it reached the gravel bed section (Fig. 3a). The bore Froude number was close to unity ($1 < \text{Fr}_1 < 1.1$) when travelling on a gravel bed. The decelerating undular bore was relatively weak, followed by a train of secondary undulations (Fig. 3b). The passage of the decelerating undular bore did not set any pebbles into upstream motion on the mobile gravel bed (Experiment VB1). Similar to the arrested bore experiments (Li and Chanson 2018), the bore deceleration and weakening were associated with a reduction in front height with further distance travelled

upstream. However, the decelerating undular bore did not stop propagating upstream of the gravel bed in the current experiments. Instead, the bore front height gradually reduced to zero, and the secondary waves disappeared as the bore front vanished (Fig. 3c).

Ensemble-statistical measurements

Free-surface measurements

A typical dataset of ensemble-median free-surface elevations d_{50} and instantaneous free-surface fluctuations d_{75-25} at different longitudinal locations are presented in Fig. 4. Herein, d_{75-25} is the difference between the 75th and 25th percentiles of the free-surface elevation ensembles, and characterizes the instantaneous free-surface fluctuations. The time $t = 0$ indicates the sudden closure of the Tainter gate, that is, the bore generation time.

As the bore propagated upstream from $x = 12$ m to $x = 3$ m, its leading edge gradually loses strength with a reduced front height. Meanwhile, the secondary wave train became barely visible (Fig. 4a). The bore-induced instantaneous free-surface fluctuations d_{75-25} showed overall smaller peak values at further upstream locations (Fig. 4b). Particularly at $x = 3$ m, the bore front was nearly flat and quasi-steady with d_{75-25} less than 1 mm. All data highlighted the decreasing strength of the bore with increasing distance from the gate. When the bore reached $x = 4$ m at a dimensionless time of approximately 325, there was no secondary undulation behind the leading edge. The free surface downstream of the bore was nearly horizontal, comparable to the M1 backwater surface profile. This phenomenon may also be predicted numerically and analytically (Li et al. 2017; Viero et al. 2017). For $x < 4$ m, the decelerating bore profile became a connection between two nearly straight free-surface sections downstream and upstream of the “bore front”. This is the vanishing bore illustrated in Fig. 3c, and its Froude number is close to unity. The shape of the vanishing bore was very similar to that observed during a 2012 field study of the Garonne River tidal bore (Reungoat et al. 2014).

Fig. 4. Time evolution of ensemble-median free-surface elevations d_{50} (a) and instantaneous free-surface fluctuations d_{75-25} (b) at different longitudinal locations in Experiment VB1 (mobile bed). Flow conditions: $Q = 0.039 \text{ m}^3/\text{s}$, $S_o = 0.0068$, $h = 63 \text{ mm}$, $Fr_1 = 1.06$ at $x = 7 \text{ m}$, $d_c = 0.085 \text{ m}$. [Colour online.]

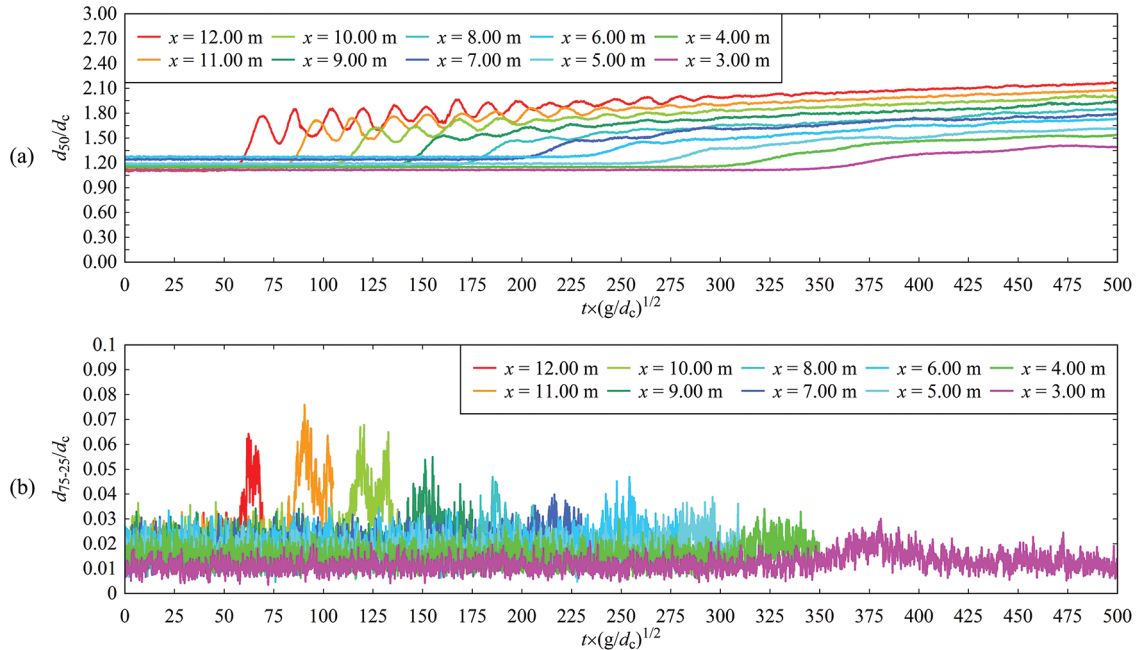
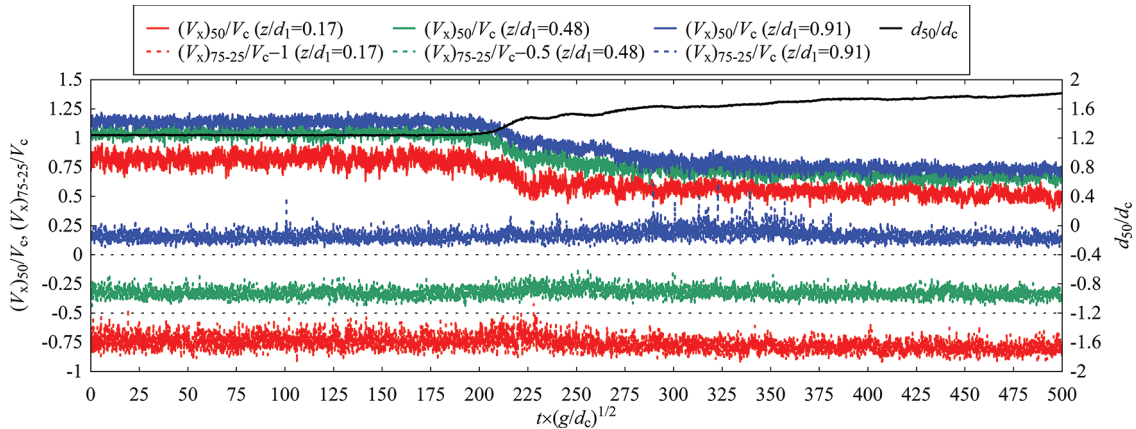


Fig. 5. Time evolution of ensemble-median flow velocity $(V_x)_{50}$ and instantaneous velocity fluctuations $(V_x)_{75-25}$ at different vertical elevations in Experiment VB1 (mobile bed). Some curves were offset vertically for better reading as indicated in the legends. Flow conditions: $Q = 0.039 \text{ m}^3/\text{s}$, $S_o = 0.0068$, $h = 63 \text{ mm}$, $Fr_1 = 1.06$ at $x = 7 \text{ m}$. [Colour online.]



Velocity measurements

A typical ensemble-averaged analysis was also conducted in terms of the median velocity components $(V_i)_{50}$ and the instantaneous velocity fluctuations $(V_i)_{75-25}$ with $i = x, y$, or z . $(V_i)_{75-25}$ is the difference between the 75th and 25th percentiles of the instantaneous velocity ensembles. The presentation of the velocity dataset is included in the Supplementary Material.¹ The ensemble-median water depth d_{50} indicates the passage of the bore at the velocity measurement location.

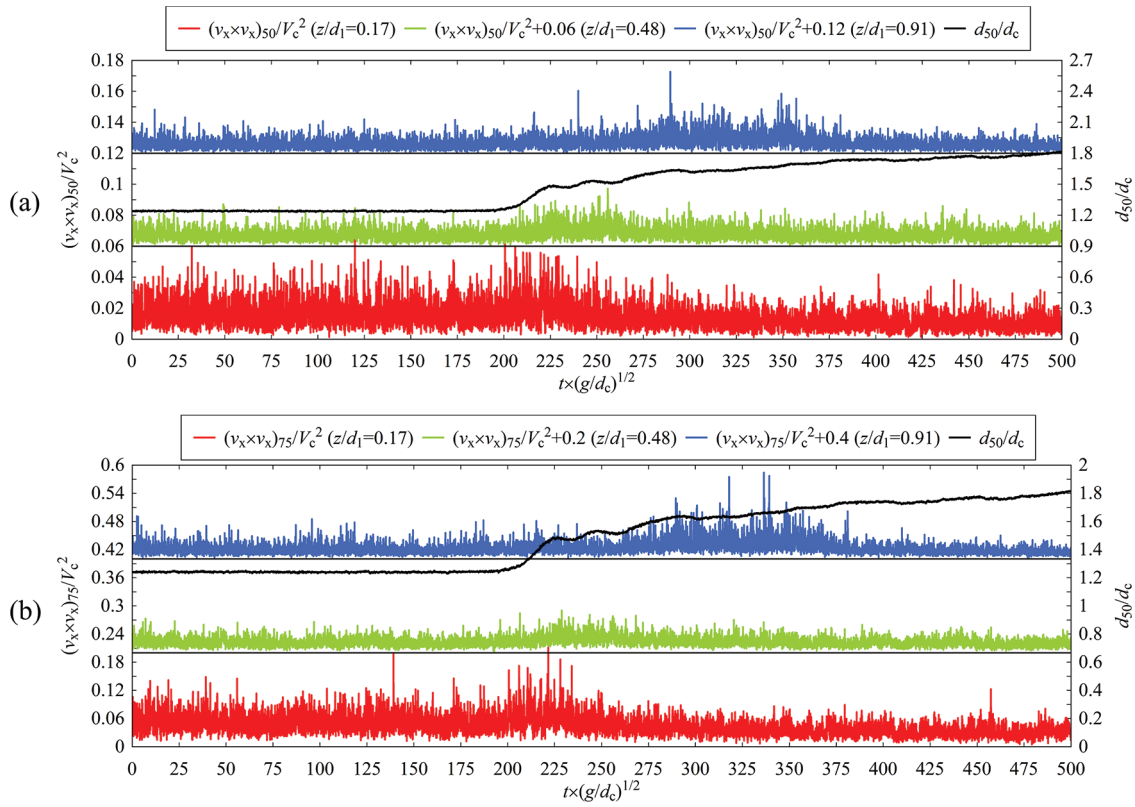
In line with previous bore experiments (Chanson 2011b; Chanson and Docherty 2012; Li and Chanson 2018), the ensemble-median longitudinal velocity component $(V_x)_{50}$ experienced a deceleration at all vertical elevations when the bore passed the ADV location (Fig. 5). No flow reversal next to the channel bed was observed

during bore passage in the current physical modelling, in contrast to some field work (Reungoat et al. 2014) and numerical simulation (Leng 2018; Lubin et al. 2010; Simon 2014). The instantaneous longitudinal velocity fluctuations $(V_x)_{75-25}$ were slightly affected by the bore arrival, and the near-bottom region experienced a rapid response, reaching a peak immediately after the bore front. The near-surface region presented enlarged $(V_x)_{75-25}$ values with a slight delay. In the 2012 field study of the Garonne River (Reungoat et al. 2014), the flat undular bore ($Fr_1 = 1.02$) induced a different change in streamwise velocity, and the surface velocity experienced a delayed reversal approximately 50 s after the bore front.

The transverse velocity data $(V_y)_{50}$ was not affected by bore arrival and oscillated about zero with the passage of the bore. The

¹Supplementary data are available with the article at <https://doi.org/10.1139/cjce-2020-0419>.

Fig. 6. Time evolution for the ensemble-median normal Reynolds stresses $(v_x \times v_x)_{50}$ (a) and the third quartile of normal Reynolds stresses $(v_x \times v_x)_{75}$ (b) at different vertical elevations in Experiment VB1 (mobile bed). Some curves were offset vertically for better reading as indicated in the legends. Flow conditions: $Q = 0.039 \text{ m}^3/\text{s}$, $S_0 = 0.0068$, $h = 63 \text{ mm}$, $Fr_1 = 1.06$ at $x = 7 \text{ m}$, $d_c = 0.085 \text{ m}$, $V_c = 0.914 \text{ m/s}$. [Colour online.]



instantaneous transverse velocity fluctuations (V_y)_{75–25} showed slightly increased disturbance from the bottom to the surface. The vertical velocity component did not experience any evident changes with bore arrival. Compared to the flat undular bore ($Fr_1 = 1.02$) documented by Reungoat et al. (2014), the current vanishing bore experiments did not show any major changes in the transverse and vertical velocity components (Fig. A-1 in the Supplementary Material).¹

Reynolds stress data

In turbulent flows, the Reynolds stress tensor $\tau_{ij} = -\rho \times v_i \times v_j$ ($i, j = x, y, z$) characterizes the shear stress on the surface area $d_x \times d_y$, $d_y \times d_z$, or $d_z \times d_x$ of the basic control volume $d_x \times d_y \times d_z$, where ρ is the fluid density, and v is the turbulent velocity fluctuation (Chanson and Docherty 2012; Pickett 1999). For a rapidly varied flow, its instantaneous velocity fluctuation can be calculated as $v = V - V_{50}$, where V is the instantaneous velocity and V_{50} is the ensemble-median of V (Bradshaw 1971; Chanson and Docherty 2012). Based on the ensemble turbulent velocity measurements, the normal Reynolds stresses $v_x \times v_x$, $v_y \times v_y$, $v_z \times v_z$, and tangential Reynolds stresses $v_x \times v_y$, $v_y \times v_z$, $v_z \times v_x$ were derived. The data of dimensionless ensemble-median Reynolds stresses and their quartile analysis results in terms of $v_x \times v_x$, $v_z \times v_z$, and $v_z \times v_x$ are illustrated in the Supplementary Material.¹

The normal stress $v_x \times v_x$ experienced some weak peak values with the bore arrival at all three vertical elevations (Fig. 6), and the third quartile data represented some characteristic larger values. In the near-bottom region, $(v_x \times v_x)_{50}$ and $(v_x \times v_x)_{75}$ were relatively smaller after the bore front passage, in comparison to those in the initially steady flow. In the near-surface area, large values of $(v_x \times v_x)_{50}$ and $(v_x \times v_x)_{75}$ were also observed during the secondary undulations after the bore front passage.

The data of $v_z \times v_z$ and $v_z \times v_x$ exhibited similar patterns in the near-surface and near-bottom elevations, although the magnitudes of the data might be unreliable because of the noise of instantaneous vertical velocity data (Figs. A-2 and A-3 in the Supplementary Material).¹

Conclusion and future work

The vanishing process of bores and positive surges in subcritical open-channel flows were modeled by laboratory experiments in a relatively large facility. Visual observations of the bore shape transformation were recorded, and quantitative measurements were performed in terms of free-surface elevation and unsteady velocity under well-controlled flow conditions.

During the upstream propagation of a weak undular bore against a subcritical inflow, the height of the leading front decreased with time until it vanished. At the late stage, the bore Froude number was close to unity, and the bore profile was nearly flat. Despite the weak strength, some increase in turbulence characteristics was still linked to the passage of the bore front, that is, free-surface fluctuations, velocity fluctuations, and Reynolds stresses.

The current study provides a benchmark dataset for the theoretical and numerical models of bores and surges at the decaying stage. Further research may be extended to the whole flow field variations underneath vanishing bores, as well as different boundary conditions, although great care is required to reproduce the vanishing bores systematically.

Disclosure statement

No potential conflict of interest is reported by the authors.

Funding

This work was supported by the Australian Research Council (DP120100481).

Acknowledgement

The authors acknowledge the technical assistance of Jason Van Der Gevel and Matthews Stewart (The University of Queensland). The helpful discussions with Dr. Xinqian (Sophia) Leng are acknowledged. The first author is grateful to the China Scholarship Council for financial support during his PhD study at The University of Queensland, Australia.

References

- Bradshaw, P. 1971. An introduction to turbulence and its measurement. Pergamon, Oxford, UK. doi:[10.1016/C2013-0-02451-6](https://doi.org/10.1016/C2013-0-02451-6).
- Chanson, H. 2011a. Tidal bores, aegir, eagre, mascaret, pororoa: theory and observations. World Scientific, Singapore. doi:[10.1142/8035](https://doi.org/10.1142/8035).
- Chanson, H. 2011b. Turbulent shear stresses in hydraulic jumps, bores and decelerating surges. *Earth Surface Processes and Landforms*, **36**(2): 180–189. doi:[10.1002/esp.2031](https://doi.org/10.1002/esp.2031).
- Chanson, H., and Docherty, N.J. 2012. Turbulent velocity measurements in open channel bores. *European Journal of Mechanics – B/Fluids*, **32**: 52–58. doi:[10.1016/j.euromechflu.2011.10.001](https://doi.org/10.1016/j.euromechflu.2011.10.001).
- Kobayashi, N., and Johnson, B.D. 2001. Sand suspension, storage, advection, and settling in surf and swash zones. *Journal of Geophysical Research: Oceans*, **106**(C5): 9363–9376. doi:[10.1029/2000JC000557](https://doi.org/10.1029/2000JC000557).
- Leng, X. 2018. A study of turbulence: the unsteady propagation of bores and surges. Ph.D thesis, School of Civil Engineering, The University of Queensland, Brisbane, Australia. doi:[10.14264/uql.2018.501](https://doi.org/10.14264/uql.2018.501).
- Li, Y. 2020. Hydrodynamics of tidal bores: turbulent propagation and sediment transport. Ph.D. thesis, School of Civil Engineering, The University of Queensland, Brisbane, Australia. doi:[10.14264/uql.2020.671](https://doi.org/10.14264/uql.2020.671).
- Li, Y., and Chanson, H. 2018. Decelerating bores in channels and estuaries. *Coastal Engineering Journal*, **60**(4): 449–465. doi:[10.1080/21664250.2018.1529261](https://doi.org/10.1080/21664250.2018.1529261).
- Li, Y., Pan, D., Chanson, H., and Pan, C. 2017. Tidal bore progressing on a small slope. *Experimental Thermal and Fluid Science*, **88**: 513–518. doi:[10.1016/j.expthermflusci.2017.07.004](https://doi.org/10.1016/j.expthermflusci.2017.07.004).
- Lubin, P., Chanson, H., and Glockner, S. 2010. Large Eddy Simulation of turbulence generated by a weak breaking tidal bore. *Environmental Fluid Mechanics*, **10**(5): 587–602. doi:[10.1007/s10652-009-9165-0](https://doi.org/10.1007/s10652-009-9165-0).
- Murty, T.S., Flather, R.A., and Henry, R.F. 1986. The storm surge problem in the bay of Bengal. *Progress in Oceanography*, **16**(4): 195–233. doi:[10.1016/0079-6611\(86\)90039-X](https://doi.org/10.1016/0079-6611(86)90039-X).
- Piquet, J. 1999. Turbulent flows: models and physics. Springer, Berlin, Heidelberg. <https://dx.doi.org/10.1007/978-3-662-03559-7>
- Reungoat, D., Chanson, H., and Caplain, B. 2014. Sediment processes and flow reversal in the undular tidal bore of the Garonne River (France). *Environmental Fluid Mechanics*, **14**(3): 591–616. doi:[10.1007/s10652-013-9319-y](https://doi.org/10.1007/s10652-013-9319-y).
- Simon, B. 2014. Effects of tidal bores on turbulent mixing: a numerical and physical study in positive surges. Ph.D. thesis, School of Civil Engineering, The University of Queensland, Brisbane, Australia. doi:[10.14264/uql.2014.19](https://doi.org/10.14264/uql.2014.19).
- St-Germain, P., Nistor, I., Townsend, R., and Shibayama, T. 2014. Smoothed-particle hydrodynamics numerical modeling of structures impacted by tsunami bores. *Journal of Waterway, Port, Coastal, and Ocean Engineering*, ASCE, **140**(1): 66–81. doi:[10.1061/\(ASCE\)WW.1943-5460.0000225](https://doi.org/10.1061/(ASCE)WW.1943-5460.0000225).
- Treske, A. 1994. Undular bores (Favre-waves) in open channels – experimental studies. *Journal of Hydraulic Research*, **32**(3): 355–370. doi:[10.1080/00221689409498738](https://doi.org/10.1080/00221689409498738).
- Viero, D.P., Peruzzo, P., and Defina, A. 2017. Positive surge propagation in sloping channels. *Water*, **9**(7): 518. doi:[10.3390/w9070518](https://doi.org/10.3390/w9070518).
- Zeng, J., Chen, G., Pan, C., and Zhang, Z. 2017. Effect of dike line adjustment on the tidal bore in the Qiantang Estuary, China. *Journal of Hydrodynamics*, **29**(3): 452–459. doi:[10.1016/S1001-6058\(16\)60756-4](https://doi.org/10.1016/S1001-6058(16)60756-4).